Anisotropic Emission from Multilayered Plasmon Resonator Nanocomposites of Isotropic Semiconductor Quantum Dots

Tuncay Ozel,[†] Sedat Nizamoglu,[†] Mustafa A. Sefunc,[†] Olga Samarskaya,[†] Ilkem O. Ozel,[†] Evren Mutlugun,[†] Vladimir Lesnyak,[‡] Nikolai Gaponik,[‡] Alexander Eychmuller,[‡] Sergey V. Gaponenko,[§,*] and Hilmi Volkan Demir[†,⊥,*]

[†]Department of Physics, Department of Electrical and Electronics Engineering, and UNAM—Institute of Materials Science and Nanotechnology, Bilkent University, TR-06800, Ankara, Turkey, [‡]Physical Chemistry, TU Dresden, Bergstrasse 66b, 01062 Dresden, Germany, [§]Stepanov Institute of Physics, National Academy of Sciences of Belarus , Minsk, 220072, Belarus, and [⊥]School of Electrical and Electronic Engineering, Division of Microelectronics, School of Mathematical and Physical Sciences, Luminous Semiconductor Lighting and Display Center of Excellence, Nanyang Technological University, Nanyang Avenue, Singapore 639798, Singapore

ABSTRACT We propose and demonstrate a nanocomposite localized surface plasmon resonator embedded into an artificial three-dimensional construction. Colloidal semiconductor quantum dots are assembled between layers of metal nanoparticles to create a highly strong plasmon—exciton interaction in the plasmonic cavity. In such a multilayered plasmonic resonator architecture of isotropic CdTe quantum dots, we observed polarized light emission of 80% in the vertical polarization with an enhancement factor of 4.4, resulting in a steady-state anisotropy value of 0.26 and reaching the highest quantum efficiency level of 30% ever reported for such CdTe quantum dot solids. Our electromagnetic simulation results are in good agreement with the experimental characterization data showing a significant emission enhancement in the vertical polarization, for which their fluorescence decay lifetimes are substantially shortened by consecutive replication of our unit cell architecture design. Such strongly plasmon—exciton coupling nanocomposites hold great promise for future exploitation and development of quantum dot plasmonic biophotonics and quantum dot plasmonic optoelectronics.

KEYWORDS: localized surface plasmons · excitons · fluorescence anisotropy · resonators · semiconductor quantum dots · layer-by-layer assembly · nanocomposites

To date extensive research has proved that metals and semiconductors exhibit extraordinary photophysical properties in nanodimensions compared to their bulk counterparts.[1] For example, an interesting effect is observed in nanostructured metals, *e.g.*, metal nanoparticles (NPs), where localized plasmon excitation results in a highly tunable optical response using the size effect. Such plasmonic effects are used in applications of biosensing,[2] light generation,[3] ultrasensitive molecular analysis by means of surface enhanced Raman spectroscopy (SERS)[4] and light harvesting.[5] Another field of interest at the nanoscale is the investigation of light generation and harvesting using colloidal semiconductor quantum dots (QDs), also known as nanocrystals, synthesized in few nanometers, with their emission and absorption excitonic peaks conveniently controllable using the quantum size effect. QDs have attracted great attention for their potential use in different applications including biological labeling and imaging,[6,7] solid-state lighting,[8−10] and photovoltaics.[11,12] The use of QDs in such applications necessitates the investigation of obtaining highly efficient QD solids and in some applications with a control over emission polarization. However, the quantum efficiency of colloidal QDs unfortunately decreases with the film formation, and the nature of the emission is highly isotropic.[13] For this, plasmon coupling of QDs provides a potential solution since the emission nature and kinetics of quantum dots can be highly modified by the oscillating plasmons of metal NPs when brought into close proximity. For example, quantum dot emission can be enhanced (or quenched) *via* plasmonic coupling as a combination of the increase in the radiative (or nonradiative) decay rates and the field localization under certain conditions. Separation between metal NPs and semiconductor QDs, spectral match between plasmon resonance wavelength of metal NPs and emission wavelength of QDs, and the geometry of metal NPs are among important conditions that affect plasmon coupling and emission modifications of QDs.

In the literature, plasmonic coupling of QDs using plasmonic metal NPs has been widely studied.[3,14−17] One of the main methods used for QD-NP plasmonic coupling is the layer-by-layer (LbL) assembly of metal

*Address correspondence to volkan@bilkent.edu.tr, s.gaponenko@ifanbel.bas-net.by.

Received for review November 9, 2010 and accepted January 7, 2011.

Published online January 19, 2011
10.1021/nn1030324

NP and quantum dot monolayers (MLs). Another important mechanism studied in the literature is the investigation of exciton−plasmon interactions to achieve polarized emission from isotropic emitters.[18,19] Previous works focused on the plasmonic coupling of only bilayers that contain the QD films located on the top or bottom of the metal NPs. Additionally, polarization dependency of the emitted light is studied only for rod-like antisymmetric metal particles, since spherically symmetric particles are expected to enhance the emission in an isotropic way.[20−22] Here, to the best of our knowledge, we propose and demonstrate the first accounts of plasmonic coupling nanocomposites of QDs in a three-dimensional construction by repeating QD-NP unit cells to successively increase the quantum efficiency of the composite film and modify the isotropic emission nature of QDs in plasmonic cavities *via* the use of repeated spherical metal NPs. These metal NP layers sandwiching QD layers on top of each other form coupled plasmon resonators that are sensitive to the polarization of incident optical excitation and result in particularly strong local field enhancements in their small gaps for the vertical polarization of excitation. The gap between metal NP layers in each plasmon resonator is intentionally selected to be small, since the generated local electric field is increased as the gap in the resonator is decreased. This is supported by our finite-difference time-domain (FDTD) simulation and is also discussed in the recent literature using theoretical calculations and computational methods.[23,24] Moreover, our simulation results show that it is possible to create nanorod-like antisymmetrical localized surface plasmons by the use of spherically symmetric Au NPs that are vertically aligned in the composite film. As a result, in our bottom-up design of these hybrid nanocomposite plasmonic resonators, the emission kinetics and the polarization nature are strongly modified, and a quantum efficiency of 30% is achieved in the composite film, which is a record for such CdTe QD solids. This artificial three-dimensional plasmon resonator approach holds great promise for the emerging quantum dot biophotonic sensor and optoelectronic device technologies to embed plasmonic NPs into nanocomposites of QDs for the demonstration of highly efficient anisotropic emitters and strong absorbers.

RESULTS AND DISCUSSION

In our study we design and construct three different unit cell architectures that are prepared using different combinations of plasmonic Au NP, isotropic CdTe QD, and dielectric spacer MLs. Representative schematics of the first, second, and third unit cell are depicted in Figure 1A−C, respectively. For the best plasmonic coupling condition, we synthesize 15 nm sized Au NPs and 5.5 nm sized CdTe QDs to spectrally match the plasmonic resonance of Au NPs to the emission

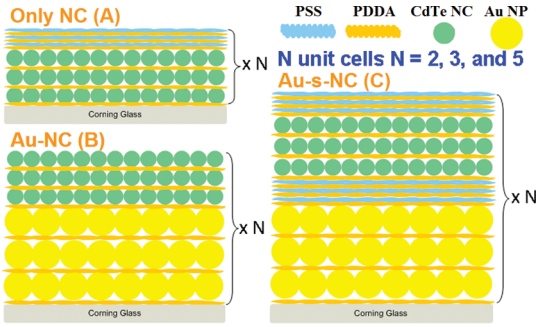

Figure 1. Schematic representations of: (A) the first unit cell that contains only CdTe QDs and PDDA/PSS dielectric spacer (denoted as only NC), (B) the second unit cell that contains Au NPs and CdTe QDs with no spacer (denoted as Au−NC), and (C) the third unit cell that contains Au NPs, CdTe QDs, and PDDA/PSS dielectric spacer (denoted as Au−s−NC), which are repeated for *N* = 2, 3, and 5 times.

peak wavelength of the QDs. Scanning electron microscopy images for water-soluble CdTe QDs and Au NPs are given in the Supporting Information. Subsequently the dielectric spacer thickness between the QDs and metal NPs is optimized by increasing bilayer dielectric thickness to obtain the maximum emission enhancement. We employ a computerized dip coater system (Nima Technology, U.K.) to construct composite films of our hybrid structures that incorporate semiconductor QDs and metal NPs in a LbL assembly by consecutive adsorption of positive poly(diallyldimethylammonium chloride) (PDDA) and negative poly(styrene sulfonate) (PSS) polymers, as described in the literature.[25,26] Following ML film formation high-precision VASE ellipsometer (J.A. Woollam Co., U.S.A.) and atomic force microscope (PSIA Inc., U.S.A.) are used in various samples to monitor the film thickness, homogeneity, and surface coverage. The first sample set is constructed with a unit cell consisting of three MLs of negatively charged QDs coated with positively charged PDDA. On top of QD layers, three bilayers of PDDA/PSS spacer (−s−) coated to serve as a dielectric spacer. This first set (named only NC) serves as the reference emission level coming only from CdTe QD solids. The second sample set (named Au−NC) consists of three MLs of Au NPs followed by coating of three MLs of QDs with no spacer layers. This set serves for the investigation of PL quenching due to the direct contact to the metal NPs. The third sample set (named Au−s−NC) consists of three MLs of Au NPs, followed by the dielectric spacer of three bilayers of PDDA/PSS, and three MLs of QDs. Here the prepared unit cells are repeated for two, three, and five times (*N* = 2, 3, and 5) in different sets of samples for a comparative study of the increased repetition of unit cells to create an increasing number of coupled plasmon resonators.

The spectral match between plasmon resonance wavelength of metal NPs and emission wavelength

of semiconductor quantum dots is among the most important conditions affecting quantum dot emission mechanisms. Therefore, in reporting the plasmon resonance condition it is important to note that the localized plasmon wavelength of these metal NPs features a strong red shift when they are assembled in film, as we show in our experimental results and well-matching numerical calculations as depicted in Figure 2. In our experiments we intentionally target for plasmonic enhancement of CdTe QD layers for on-resonance condition. This type of on-resonance coupling has commonly been reported in the previous works for different kinds of metal nanostructures and quantum dots.[3,14−16,27] (Although there is one prior report of plasmonic enhancement of CdTe QD layer by the use of Au NPs in a two-dimensional system for off-resonance spectral conditions.)[17]

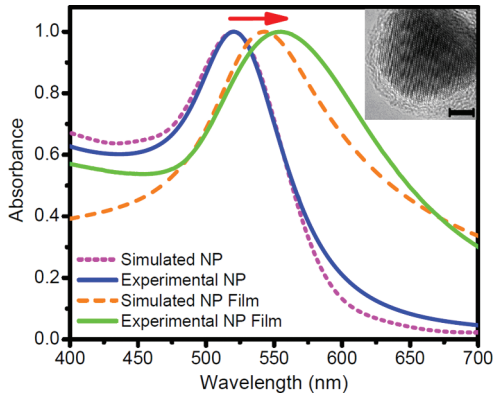

Figure 2. Normalized absorbance spectra of Au NPs: (magenta-dotted) simulation result of isolated particles, (blue-solid) experimental result of isolated particles, (orange-dashed) simulation result of assembled particles inside a dielectric medium, (green-solid) experimental result of LbL assembled particles in a dielectric medium. Inset is a high-resolution transmission electron (HRTEM) microscope image of a single Au NP. The scale bar is 3 nm.

Here we experimentally find out that three MLs of PDDA/PSS bilayers make the optimal dielectric spacing for the enhancement of QD emission in our case. Enhancement factor is measured to be <2 for one unit cell. This enhancement factor is not very high compared to some of the previous reports since we start with highly efficient quantum dot solids (19%), where those previously demonstrated plasmon coupled quantum dot solids typically have initial efficiency of only a few percent. The room for photoluminescence enhancement inversely depends on the starting quantum efficiency of the quantum dots as described in the literature[28] (and can be easily driven from eqs 3 and 4 discussed later in the paper). The consequence of these two equations is that it is possible to obtain much higher enhancement factors by the use of quantum dots with very low efficiency levels.

Photoluminescence spectra of two-, three-, and five-times repeated unit cells of Au NP and CdTe QD nanocomposite films are depicted in Figure 3A−C, respectively. We observe that, in the presence of metal NPs separated by the dielectric layer, QD emission is substantially enhanced. But in the presence of metal NPs lacking a dielectric spacer, QD emission is quenched. We calculate that the QD emission is enhanced by a

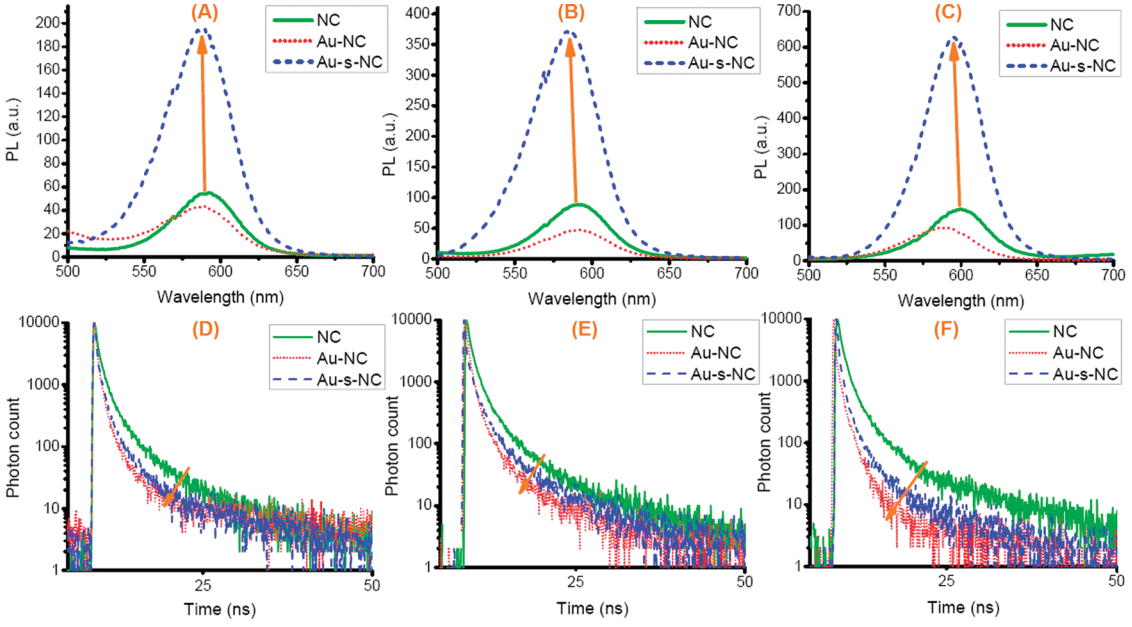

Figure 3. Photoluminescence spectra of CdTe QDs alone (NC) and those in the presence of Au NPs (Au−NC) and in the presence of Au NPs and PDDA/PSS dielectric spacer (Au−s−NC) with their corresponding CdTeQD−Au NP unit cells repeated for: (A) two, (B) three, and (C) five times in the composite. Inset figures correspond to each sample layer designs with arrows representing the plasmon-exciton interactions. Time-resolved photoluminescence decays of our CdTe QDs alone (NC) and those in the presence of Au NPs (Au−NC) and in the presence of Au NPs and PDDA/PSS dielectric spacer (Au−s−NC) with their unit cells repeated for: (D) two, (E) three, and (F) five times.

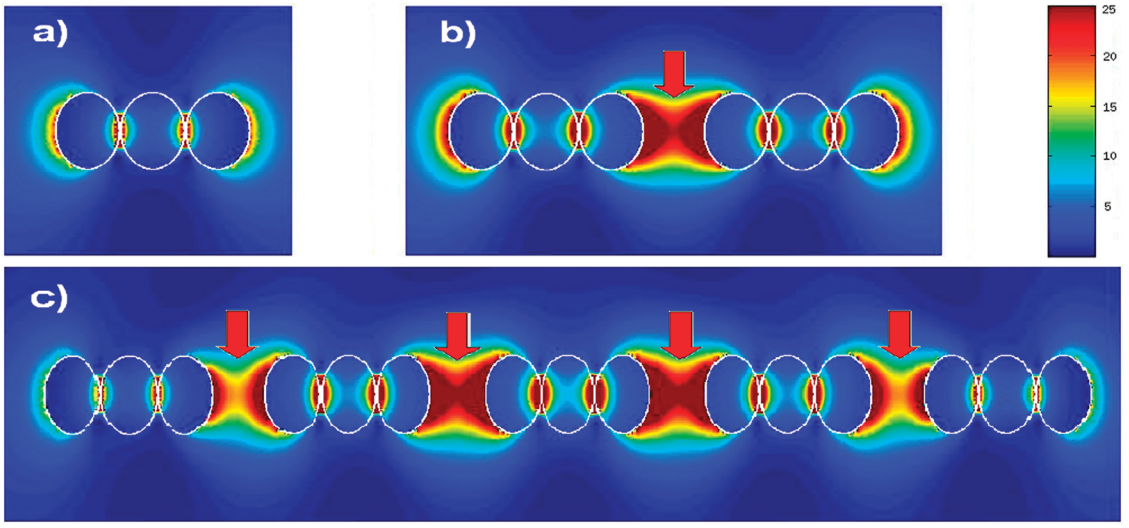

Figure 4. Electric field map distribution of: (A) one-, (B) two-, and (C) five-times repeating horizontally aligned three Au NPs (circled in white for easy recognition) of 15 nm diameter illuminated with an incident plane-wave radiating at 612 nm, propagating along the *y*-axis and polarized along the *x*-axis source (arrows indicate the intense electric field due to coupled plasmon resonators). (Note that the field maps shown here are rotated by 90° with respect to the orientation of the composite film samples, for which the horizontally side-by-side metal nanospheres depicted here correspond to vertically aligned NPs in the composite film.)

factor of 3.6 with a two-time unit cell repetition. A unit cell repetition of three times results in an enhancement factor of 4.1. For five-time repeated unit cells, the highest emission enhancement is observed with a factor of 4.4. We use an integrated sphere that is connected to an optical powermeter and an optical spectrum analyzer to observe the change in the emission characteristics of these composite samples. Using this setup, we measure the starting quantum efficiency of our QD films alone to be 19%. In the case of Au−CdTe nanocomposite films, using Au NPs at the fixed optimal dielectric spacing, we increase the film quantum efficiency to the highest level of 30% by repeating the unit cells five times, which is the largest quantum efficiency reported for CdTe QDs in film in the literature, to the best of our knowledge. This corresponds to a quantum efficiency enhancement of 63%.

Emission kinetics of these nanocomposite samples are comparatively investigated using time-resolved fluorescence decay curves, as presented in Figure 3D−F, which clearly shows strong modification as a result of plasmon coupling. Fluorescence lifetimes are measured using a time-correlated single photon counting system (Picoquant-FluoTime200) at 16 ps resolution with an excitation laser at 375 nm. Decay curves are modeled using multiexponential fit with deconvolution of the instrument response function and the intensity averaged lifetimes are reported (decay model and function are in given in the Supporting Information). We observe a significant shortening of photoluminescence decay lifetimes for each set of Au NP and CdTe QD films. For the largest modification observed in the sample of unit cells repeated for five times, the photon decay lifetime of CdTe QDs is modified from 7.9 to 1.8 ns in the presence of metal NPs and to 2.8 ns in the presence of metal NPs separated with dielectric layers, which corresponds to the strongest emission enhancement. Photoluminescence and time-resolved fluorescence characteristics support each other. In both cases with metal NPs, the total decay rates (which have both radiative and nonradiative components) are observed overall to increase. Here their modified photoluminescence spectra can be explained by a dominating increase in the nonradiative decay rate in the presence of metal NPs (with no dielectric spacer), which results in quenched fluorescence, and by a dominating increase in the radiative decay rate in the presence of metal NPs separated by dielectric layers, which results in enhanced fluorescence, with the combination of enhanced local electric fields in the close proximity of plasmon coupled QDs. It is noteworthy that the modification of emission kinetics is observed to increase with the repeating number of unit cells because the number of Au NP plasmonic cavities is increased with the unit cell number.

Our FDTD calculations (using Lumerical Solutions Inc., Vancouver, Canada) show that increased number of metal NP layers results in stronger localization of electric field between each triple NP, as depicted in Figure 4. Here each Au NP triple represents three MLs of Au NPs that are present in each unit cell (each NP in simulation represents a layer). In the presence of one unit cell electric field intensity decays exponentially with distance as depicted in Figure 4A. In the case of two and five unit cells, the electric field intensity is increased, and the field is elongated through their separation as depicted in Figure 4B and C. Such

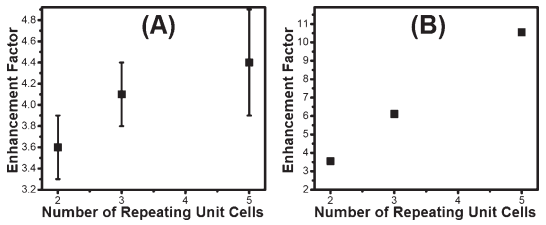

Figure 5. (A) Experimental enhancement of the quantum dot emission intensity because of the increased number of plasmon resonators as a function of the repeated number of unit cells, and (B) simulated enhancement factors derived from the calculated decay rates for two-, three-, and five-time repeating unit cell structures compared to a single unit cell structure using numerical simulations.

coupled metal NP layers serve as plasmonic resonators in which CdTe quantum dot layers are strongly plasmon coupled in this small separation (of less than 40 nm in our case).

To imitate CdTe QDs as a dipole source with the right emission wavelength center and span, our experimental photoluminescence data are used in our simulations. This dipole source is separated by 7.5 nm from Au NP triples. Using the radiated powers in the presence and the absence of metal NPs for two-, three-, and five-time repeating unit cell structures, we also calculated expected emission enhancement factors numerically. A plot of enhancement factors of experimental and numerical simulation results is depicted in Figure 5. In our numerical results we observe a linear increase in emission as the number of repeating unit cells increases (for small numbers of cells). We observe a similar increase in our experimental emission intensities, however, the trend is not linear and the enhancement factors are less than the simulation results for more than three repeating unit cell structures. This can be explained by the loss of surface roughness in the experimental sample in the presence of lots of unit cells corresponding to formation of tens of ML films.

Fluorescence anisotropy measurements of quantum dot emission are taken using a polarizer integrated time-correlated single photon counting system (Picoquant-FluoTime200) with external high-precision filters at an excitation laser wavelength of 375 nm, following a similar procedure by Kapusta *et al.*[29] with the integration of two polarizers for both excitation source and detection optics. Excitation laser is oriented in the vertical polarization with respect to the film sample under test, and both vertical and horizontal components of the emitted light are collected using the same experimental conditions. To compensate for the detection system sensitivities in different polarization orientations, the above measurements are performed with an excitation laser in the horizontal polarization (the experimental setup is further explained in detail in the Supporting Information). Correction factors (*G*-factors) are calculated using the ratio of collected emission intensities in different polarizations as given in eq 1:

$$G = \frac{I_{HV}}{I_{HH}} \tag{1}$$

The time-resolved fluorescence decay curves are integrated over time, and we calculated that 80% of the enhanced emission is in vertical polarization. Also fluorescence anisotropy of the system is calculated by the use of Picoquant FluoFit software that comes with the time-resolved setup and the steady-state anisotropy value of the CdTe quantum dots films estimated as

$$r = \frac{I_{VV} - G \cdot I_{VH}}{I_{VV} + 2 \cdot G \cdot I_{VH}} \tag{2}$$

increased from 0.02 to 0.26 when they are embedded in the plasmon resonator nanocomposite structure. The fluorescence anisotropy parameter *r* can vary between −0.2 and 0.4 for single photon processes depending on the polarization components of emitted photons. We attribute the anisotropic emission from this artificial three-dimensional film construction to the plasmon resonator structures in the film. In this architecture individual metal spheres (triple Au NPs) are attached to each other in very short distances of less than 1 nm, and they act together as Au nanorods as we observed very similar simulation results using half sphere end cylindrical structures (the simulations are given in the Supporting Information). Local field enhancement in vertical polarization results in preferential excitation of absorption transition vectors of the emitters which consequently affect the polarization degree of the emitted photons from the system. Structural estimation is supported by atomic force microscopy (AFM) images for three ML Au NPs film in which Au NPs are well separated from each other in the *x*−*y* plane, whereas they are on top of each other in a vertical z-direction (some with two particles and some with three particles vertically on top of each other).

Overall emission enhanced as a result of the repeating unit resonator structures can be further investigated by the comparison of quantum dot decay rate with and without Au NPs. For quantum dots the quantum yield can be expressed in terms of the ratio of radiative decay rate to total photoluminescence decay rate including both radiative and nonradiative decay components given in eq 3:

$$Q_0 = \frac{\Gamma}{\Gamma + k_{nr}} \tag{3}$$

where Γ is the radiative decay rate and k_{nr} is the nonradiative decay rate. In the presence of metal NPs, radiative and nonradiative components are modified, and the resulting quantum yield is given in eq 4:

$$Q_m = \frac{\Gamma + \Gamma_m}{\Gamma + \Gamma_m + k'_{nr}} \tag{4}$$

where Γ is the radiative decay rate, Γ_m is the modified radiative decay rate in the presence of metal NP, and k'_{nr} is the modified nonradiative decay rate in the presence of metal NPs. We report intensity averaged decay lifetimes for our quantum dots that are fit using multiexponentional decay analysis (given in detail in the Supporting Information). Using decay lifetimes of 7.9 ns for the quantum dots and 2.8 ns in the presence of metal NPs, we calculated Γ_m to be 0.23 ns^{-1}. Also by the use of the initial quantum yield (0.19) of quantum dot layers, the radiative decay rate is calculated to be 0.024 ns^{-1}. Finally, the quantum yield is calculated to be 0.68 in the presence of Au NPs. This corresponds to 3.6-fold enhancement in terms of quantum yield comparison. This enhancement factor is in good relation with the experimentally observed enhancement factor of 1.6 under the steady-state conditions.

In conclusion, we modified the emission characteristics of semiconductor CdTe quantum dot films by construction of repeating layers in an artificial three-dimensional plasmon resonator embedded composite structure and presented our numerical and experimental results. In the five-times repeating unit cell structure of Au NPs and CdTe quantum dot nanocomposite film separated by a dielectric layer, emission lifetime of QDs was reduced, emitted light became anisotropic, emission was enhanced by a factor of 4.4, and quantum efficiency reached a level of 30% in film. This concept of three-dimensional plasmon coupled quantum dot nanocomposites paves a new path for biosensors and highly efficient devices in nanophotonics.

METHODS

Colloidal Synthesis of CdTe Quantum Dots. Here we followed a similar synthesis procedure described by Rogach *et al.*[30] In Step 1, we prepare a 0.2 L of Milli-Q water solution with 4.59 g $Cd(ClO_4)_2$. In Step 2, we prepare a solution of 1.31 g thioglycolic acid (TGA) with Milli-Q water and complete the total amount of volume in Step 1 (0.2 L) and Step 2 (0.3 L) to make a total of 0.5 L. In Step 3, we set the solution pH to be 12 by adding 1 M NaOH under vigorous stirring of the solution. In Step 4, we let argon flow into the flask. In Step 5, 0.8 g Al_2Te_3 is put into a second flask in a glovebox. In Step 6, a solution of 10 mL of 0.5 M H_2SO_4 and 15 mL Milli-Q water is prepared. The second flask is connected to the main flask, 10 mL of Step 6 solution is added slowly into the second flask containing Al_2Te_3, and argon is used as the carrier gas during the reaction. After 30 min, the Al_2Te_3 line is removed from the system, and the cooler is connected. Heater is set to be 100 °C. Quantum dots start to grow as the mixture starts boiling and gets bigger in size during the reaction, which leads to a red shift in the emission spectrum. This procedure results in negatively charged CdTe QDs.

Colloidal Synthesis of Au NPs. In Step 1, 0.08 g of chloroauric acid $HAuCl_4$ is dissolved in 200 mL of Milli-Q water corresponding to a molarity of 1 mM. In Step 2, 0.26 g of trisodium citrate $Na_3C_6H_5O_7$ is dissolved in 20 mL of Milli-Q water corresponding to a molarity of 44 mM in another beaker. Under continuous stirring, the first beaker is heated up until it starts boiling. Preheated trisodium citrate solution in the second beaker is added quickly into the first beaker. The mixture is kept boiling for 20−30 min to obtain stable dark-red-colored gold NPs with an average diameter of 15 nm. Finally, the mixture is cooled down to room temperature under continuous stirring.

Layer by Layer Film Construction. Two mg/mL of positively charged polymer, PDDA dissolved in 0.1 M NaCl solution, was used for coating on negatively charged pretreated Corning glasses and for forming all LbL constructions with CdTe QDs and Au NPs. PSS is used as the complementary negatively charged polymer with the concentration of 2 mg/mL dissolved in 0.1 M NaCl solution, for dielectric spacing construction.

FDTD Calculations. In this paper, the simulations are carried out by using the finite difference time domain (FDTD) method. We performed our simulations in a commercial software package (Lumerical Solutions Inc., Vancouver, Canada). In our simulations we used Johnson and Christy[31] data which have a perfect match with dielectric behavior of our colloidally synthesized Au NPs. A propagating plane wave was introduced into the simulation region to replicate the electromagnetic wave in the experiment. To observe the plasmonic response of Au NPs, we set the planewave options to create an electric field parallel to the Au NPs layer. The diameter value of each Au NP is set to be 15 nm. These NPs are integrated into a medium with a refractive index of 1.4 (which corresponds to the refractive index of PDDA: PSS) to set up the same surrounding conditions in the experiment. FDTD simulations are done to imitate the response of Au NPs in solution and also in film. Enhancement factor calculations are carried out by the use of transmission and radiation intensity calculations in the absence and the presence of Au NPs in close proximity to a dipole source (to imitate quantum dots in our experiments). The simulation region is divided into 0.1 nm mesh size to minimize the staircase effect on the boundaries of metal spheres.

Acknowledgment. The authors thank P. Kapusta and K. Aydin for their fruitful comments on anisotropy measurements and FDTD simulations. This work is supported by NRF-RF-2009-09, EU-FP7 Nanophotonics4Energy NoE, BMBF TUR 09/001, and TUBITAK EEEAG 106E020, 107E297, 107E088, 109E002, 109E004, 110E010, and 110E217. H.V.D. acknowledges support from ESF-EURYI and TUBA-GEBIP.

Supporting Information Available: Electric field intensity maps of Au nanorods with semispherical ends, AFM image for three ML Au NP-coated samples, more characterization results of synthesized materials, and illustration of optical setups for anisotropy and *G*-factor measurements. This material is available free of charge *via* the Internet at http://pubs.acs.org.

REFERENCES AND NOTES

1. Gaponenko, S. V. *Introduction to Nanophotonics*; Cambridge University Press: Cambridge, U.K., 2010.
2. Anker, J. N.; Hall, W. P.; Lyandres, O.; Shah, N. C.; Zhao, J.; Van Duyne, R. P. Biosensing with Plasmonic Nanosensors. *Nat. Mater.* **2008,** *7*, 442–453.
3. Pompa, P. P.; Martiradonna, L.; Torre, A. D.; Sala, F. D.; Manna, L.; Vittorio, M. D.; Calabi, F.; Cingolani, R.; Rinaldi, R. Metal-enhanced Fluorescence of Colloidal Nanocrystals with Nanoscale Control. *Nat. Nanotechnol.* **2006,** *1*, 126–130.
4. Gaponenko, S. V.; Guzatov, D. V. Possible Rationale for Ultimate Enhancement Factor in Single Molecule Raman Spectroscopy. *Chem. Phys. Lett.* **2009,** *477*, 411–414.
5. Atwater, H. A.; Polman, A. Plasmonics for Improved Photovoltaic Devices. *Nat. Mater.* **2010,** *9*, 205–213.
6. Gao, X.; Cui, Y.; Levenson, R. M.; Chung, L. W. K.; Nie, S. *In Vivo* Cancer Targeting and Imaging with Semiconductor Quantum Dots. *Nat. Biotechnol.* **2004,** *22*, 969–976.
7. Medintz, I. L.; Uyeda, H. T.; Goldman, E. R.; Mattoussi, H. Quantum Dot Bioconjugates for Imaging, Labelling and Sensing. *Nat. Mater.* **2005,** *4*, 435–446.

8. Gaponenko, S. V. *Optical Properties of Semiconductor Nanocrystals*; Cambridge University Press: Cambridge, U.K., 2005.
9. Sun, Q.; Wang, Y. A.; Li, L. S.; Wang, D.; Zhu, T.; Xu, J.; Yang, C.; Li, Y. Bright, Multicoloured Light-emitting Diodes Based on Quantum Dots. *Nat. Photonics* **2007,** *1*, 717–722.
10. Nizamoglu, S.; Ozel, T.; Sari, E.; Demir, H. V. White Light Generation Using CdSe/ZnS Core-Shell Nanocrystal Hybridized with InGaN/GaN Light Emitting Diodes. *Nanotechnology* **2007,** *18*, 065709.
11. Huynh, W. U.; Dittmer, J. J.; Alivisatos, A. P. Hybrid Nanorod-Polymer Solar Cells. *Science* **2002,** *295*, 2425–2427.
12. Mutlugun, E.; Soganci, I. M.; Demir, H. V. Photovoltaic Nanocrystal Scintillators Hybridized on Si Solar Cells for Enhanced Conversion Efficiency in UV. *Opt. Express* **2008,** *16*, 3537–3545.
13. Chistyakov, A. A.; Martynov, I. L.; Mochalov, K. E.; Oleinikov, V. A.; Sizova, S. V.; Ustinovich, E. A.; Zakharchenko, K. V. Interaction of CdSe/ZnS Core-Shell Semiconductor Nanocrystals in Solid Thin Films. *Laser Phys.* **2006,** *16*, 1625–1632.
14. Kulakovich, O.; Strekal, N.; Yaroshevich, A.; Maskevich, S.; Gaponenko, S.; Nabiev, I.; Woggon, U.; Artemyev, M. Enhanced Luminescence of CdSe Quantum Dots on Gold Colloids. *Nano Lett.* **2002,** *2*, 1449–1452.
15. Shimizu, K. T.; Woo, W. K.; Fisher, B. R.; Eisler, H. J.; Bawendi, M. G. Surface-enhanced Emission from Single Semiconductor Nanocrystals. *Phys. Rev. Lett.* **2002,** *89*, 117401.
16. Fedutik, Y.; Temnov, V. V.; Schops, O.; Woggon, U.; Artemyev, M. V. Exciton-Plasmon-Photon Conversion in Plasmonic Nanostructures. *Phys. Rev. Lett.* **2007,** *99*, 136802.
17. Komarala, V. K.; Rakovich, Y. P.; Bradley, A. L.; Byrne, S. J.; Gun'ko, Y. K.; Gaponik, N.; Eychmüller, A. Off-resonance Surface Plasmon Enhanced Spontaneous Emission from CdTe Quantum Dots. *Appl. Phys. Lett.* **2006,** *89*, 253118.
18. Lakowicz, J. R.; Malicka, J.; Gryczynski, I.; Gryczynski, Z. Directional Surface Plasmon-coupled Emission: A New Method for High Sensitivity Detection. *Biochem. Biophys. Res. Commun.* **2003,** *307*, 435–439.
19. Aslan, K.; Lakowicz, J. R.; Geddes, C. D. Metal-enhanced Fluorescence Using Anisotropic Silver Nanostructures: Critical Progress to Date. *Anal. Bioanal. Chem.* **2005,** *382*, 926–933.
20. Ming, T.; Zhao, L.; Yang, Z.; Chen, H.; Sun, L.; Wang, J.; Yan, C. Strong Polarization Dependence of Plasmon-Enhanced Fluorescence on Single Gold Nanorods. *Nano Lett.* **2009,** *9*, 3896–3903.
21. Mertens, H.; Biteen, J. S.; Atwater, H. A.; Polman, A. Polarization-Selective Plasmon-Enhanced Silicon Quantum-Dot Luminescence. *Nano Lett.* **2006,** *6*, 2622–2625.
22. Bouhelier, A; Bachelot, R.; Lerondel, G.; Kostcheev, S.; Royer, P.; Wiederrecht, G. P. Surface Plasmon Characteristics of Tunable Photoluminescence in Single Gold Nanorods. *Phys. Rev. Lett.* **2005,** *95*, 267405.
23. Sondergaard, T.; Jung, J.; Bozhevolnyi, S. I.; Della Valle, G. Theoretical Analysis of Gold Nano-strip Gap Plasmon Resonators. *New J. Phys.* **2008,** *10*, 105008.
24. Muskens, O. L.; Giannini, V.; Sanchez-Gil, J. A.; Gomez Rivas, J. Optical Scattering Resonances of Single and Coupled Dimer Plasmonic Nanoantennas. *Opt. Express* **2007,** *15*, 17736–17746.
25. Decher, G. Fuzzy Nanoassemblies: Toward Layered Polymeric Multicomposites. *Science* **1997,** *277*, 1232–1237.
26. Gaponik, N. Assemblies of Thiol-capped Nanocrystals as Building Blocks for Use in Nanotechnology. *J. Mater. Chem.* **2010,** *20*, 5174–5181.
27. Ozel, T.; Soganci, I. M.; Nizamoglu, S.; Huyal, I. O.; Mutlugun, E.; Sapra, S.; Gaponik, N.; Eychmüller, A.; Demir, H. V. Selective Enhancement of Surface-State Emission and Simultaneous Quenching of Interband Transition in White-Luminophor CdS Nanocrystals Using Localized Plasmon Coupling. *New J. Phys.* **2008,** *10*, 083035.
28. Gersten, J.; Nitzan, A. Spectroscopic Properties of Molecules Interacting with Small Dielectric Particles. *J. Chem. Phys.* **1981,** *75*, 1139–1152.
29. Kapusta, P.; Erdmann, R.; Ortmann, U.; Wahl, M. Time-resolved Fluorescence Anisotropy Measurements Made Simple. *J. Fluoresc.* **2003,** *13*, 179–183.
30. Rogach, A. L.; Franzl, T.; Klar, T. A.; Feldmann, J.; Gaponik, N.; Lesnyak, V.; Shavel, A.; Eychmüller, A.; Rakovich, Y. P.; Donegan, J. F. Aqueous Synthesis of Thiol-Capped CdTe Nanocrystals: State-of-the-Art. *J. Phys. Chem. C* **2007,** *111*, 14628–14637.
31. Johnson, P. B.; Christy, R. W. Optical Constants of the Noble Metals. *Phys. Rev. B: Solid State* **1972,** *6*, 4370–4379.